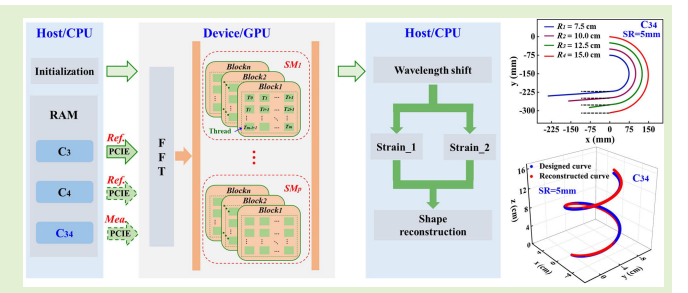


Fast Shape Reconstruction Based on GPU Parallel Computation in Optical Frequency Domain Reflectometry

Rongyi Shan, Yanjie Meng[®], Huajian Zhong, Wenfa Liang, Shuai Xiao, Yuhao Kong, Zhenwei Peng, Zhicai Zhang, Changrui Liao[®], *Member, IEEE*, Cailing Fu[®], and Yiping Wang[®], *Senior Member, IEEE*

Abstract—A fast shape reconstruction optical frequency domain reflectometry (OFDR) system that employs graphics processing unit (GPU) to parallelly calculate the cross correlation wavelength shift of the two outer cores of a standard multicore fiber (MCF) was proposed and demonstrated. The effect of the number of threads in each block on the time consumption was studied. The consumption time was 50.86 ms, when the simulated data size and the number of threads per block were 10 MS and 256, respectively. Compared to the serial computing with CPU, the time consumption was reduced by nearly 21 times for 2-D and 3-D fast shape sens-



ing. At the spatial resolution of 5 mm, the maximum reconstruction errors for 2-D and 3-D shape sensing were 3.23% and 2.47%, respectively, with MCF lengths of 47.1 and 43.6 cm.

Index Terms—Multicore fiber (MCF), optical frequency domain reflectometry (OFDR), parallel processing algorithm, shape reconstruction.

I. INTRODUCTION

PIBER shape sensors based on multicore fiber (MCF) [1], [2], [3] and fiber clusters [4], [5] have attracted attention in fields, such as interventional therapy [6], aerospace engineering [7], and structural health monitoring [8] due to their ability to track the shape and position of dynamic objects without visual contact [9]. Among them, the majority of shape sensors are using wavelength-division multiplexing fiber Bragg gratings (FBGs), whose sensing spatial resolution is limited by grating spacing [10]. In contrast, shape sensor

Received 14 August 2024; revised 13 September 2024; accepted 13 September 2024. Date of publication 23 September 2024; date of current version 31 October 2024. This work was supported in part by the National Key Research and Development Program of China under Grant 2022YFE0111400; in part by the National Natural Science Foundation of China under Grant U22A2088, Grant 62375178, and Grant 62122057; in part by Shenzhen Key Laboratory of Ultrafast Laser Micro/Nano Manufacturing under Grant ZDSYS20220606100405013; in part by Shenzhen Science and Technology Program under Grant JCYJ20220818095800001; in part by LingChuang Research Project of China National Nuclear Corporation under Grant CNNC-LCKY-202265, xx; and in part by China Postdoctoral Science Foundation under Grant 2024M752106, Grant GZC20231715, Grant 2024M752107. The associate editor coordinating the review of this article and approving it for publication was Dr. Nageswara Lalam. (Corresponding author: Yiping Wang.)

Please see the Acknowledgment section of this article for the author

Digital Object Identifier 10.1109/JSEN.2024.3462463

based on optical frequency domain reflectometry (OFDR) with MCF has become the most promising sensor due to its high spatial resolution [11]. Currently, the demand for fast shape reconstruction is increasing rapidly in many fields. However, the traditional cross correlation method that obtains the strain distribution of each core, i.e., Rayleigh backscattering (RBS) shift between the measurement and reference RBS, is a time-consuming operation with a large data size. To achieve fast strain sensing, various methods have been proposed and demonstrated. Zhou et al. [12] proposed a time-resolved OFDR that divided the overall sweep range into several equal subsections for fast strain sensing, where the measurement rate was up to 50 Hz with a spatial resolution of 20 cm. A joint algorithm of wavelength domain differential accumulation and local cross correlation was also proposed for fast strain measurement, which increased the processing speed by 6.4 times on a 113.3-m-long fiber [13]. In addition, a phase dehopping filtering differential phase strain demodulation method was applied to fast shape sensing, where the shape reconstruction speed is improved from 940 to 104 ms, i.e., nearly ten times [14]. Although afore-adopted algorithms could be used to achieve fast strain sensing, the data processing remains a challenge. Fortunately, the data processing rate for distributed optical fiber sensing could be effectively accelerated by the parallel computing in graphics

processing unit (GPU), attributing to its large number of parallel computing units. The intrinsic superiority of GPU parallel computation in phase-sensitive optical time domain reflectometer for improving the data processing capability was analyzed [15]. Subsequently, the GPU was used to accelerate the data processing rate of OFDR wide strain measurement to 800 Hz [16]. Moreover, the total process time of parallel computing in GPU was enhanced about 81 times compared to serial computing in CPU for real-time distributed dynamic OFDR strain sensing [17]. Thus, the data processing could be indeed accelerated by GPU.

In this letter, a GPU-based fast shape reconstruction OFDR system was demonstrated, which uses a GPU to parallelly calculate the cross correlation wavelength shift of the two outer cores of the MCF. The process of calculating cross correlation wavelength shift and effect of spatial resolution on the time consumption using CPU and GPU were compared, and ten kernel functions were constructed in the GPU. Moreover, the effect of the number of threads in a block on occupancy rate and time consumption was analyzed. The sensing properties, including time consumption and reconstruction error, of 2-D and 3-D shapes were further investigated by using GPU-based OFDR.

II. EXPERIMENTAL SETUP AND METHODS

The experimental setup for GPU-based fast shape reconstruction using conventional OFDR and MCF is illustrated in Fig. 1(a). As shown in the inset of Fig. 1(a), the diameter of the employed MCF is 125 μ m, and the distance between the central core, i.e., Core₇ (C_7), and the outer core is 35 μ m (SM7C1500, Fibercore Inc.). The output light from a tunable laser source (TLS, N7776C, Keysight) was divided into two parts, i.e., the auxiliary interferometer (AI) in the upper part and the main interferometer (MI) in the lower part, via a 10:90 optical coupler (OC₁). The sweeping range and sweeping rate of the TLS were 1525-1575 nm and 150 nm/s, respectively; 10% of the light was sent to AI of a Michelson interferometer, which was consisted of a delay fiber and two Faraday rotating mirror (FRM, Thorlabs), i.e., FRM₁ and FRM₂. Note that the length of delay fiber was 21.6 m. The signal generated by a balanced photodetector (BPD₁, PDB480C-AC, Thorlabs) was used as external clock signal for data acquisition card (DAQ, PCI 6115, NI) to sample the equidistant instantaneous optical frequency points and suppress the nonlinear sweep effect of the TLS; 90% of the light was sent to MI of a Mach–Zehnder interferometer and split into two beams through a 50:50 OC₂, i.e., the reference light passed through a polarization controller (PC) and the measurement light passed through an MCF with a length of 6.24 m. Then, the RBS from the MCF is mixed with the reference light by OC₄. Two polarization beam splitters, i.e., PBS₁ and PBS₂, were used to divide the mixed light into two orthogonal polarization states, i.e., P-polarization and S-polarization, which are received by two BPDs, i.e., BPD₂ and BPD3, respectively, to reduce the polarization fading effect. Note that only the P-polarization signal was used to achieve shape reconstruction, and the bandwidth of BPD and the sampling rate of DAQ were 1.6 GHz and 10 MS/s, respectively. Ultimately, the signal collected by

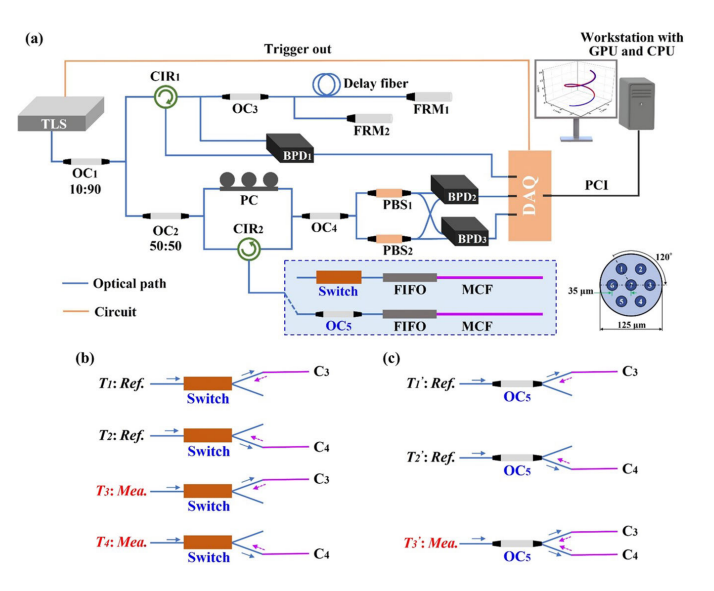
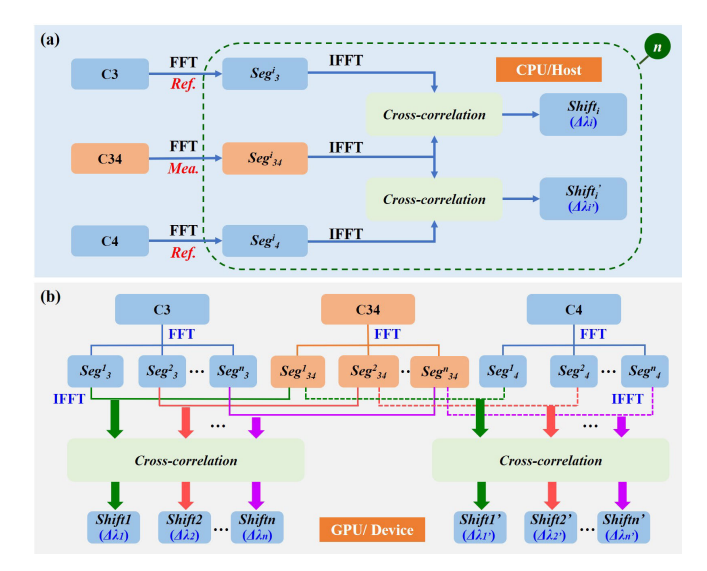


Fig. 1. (a) Experimental setup for GPU-based fast 3-D shape reconstruction using OFDR and MCF; workflow diagram of RBS signal acquisition using (b) optical switch and (c) optical coupler (OC). TLS: tunable laser source; CIR: circulator; FRM: Faraday rotating mirror; PC: polarization controller; PBS: polarization beam splitter; BPD: balanced photodetector; DAQ: data acquisition card; PCI: peripheral component interconnect; CPU: central processing unit; FIFO: fan-in-fan-out. Inset: schematic of MCF end face.

DAQ and transferred to the workstation by peripheral component interconnect (PCI). The workstation was used for signal processing, consisting of a CPU (i7-12700KF, Intel Inc.) with a floating-point peak computing power of 691.2 G floating-point operations per second (GFLOPS) and a clock rate of 3.6 GHz, as well as a GPU (NVIDIA GeForce RTX 3070 Ti, NVIDIA Inc.) with a floating-point peak computing power of 21750 GFLOPS and a clock rate of 1.58 GHz. Note that the accessible random access memory (RAM) of the CPU and GPU are 32 and 8 GB, respectively, while the RAM access speed of CPU is 4.8 GHz.

According to [1], the fiber shape could be reconstructed based on the combination of Core₃, i.e., C₃, and Core₄, i.e., C₄, using vector projections method. As shown in Fig. 1(b), the workflow of using the mechanical optical switch to acquire the RBS signal of C₃ and C₄ is listed as follows. The signals of C₃ and C₄, i.e., reference (Ref.) signals, were collected separately at time of T_1 and T_2 , respectively, when the MCF was straight, i.e., without strain. Similarly, the measurement (Mea.) signals of C_3 and C_4 were also collected at time of T_3 and T_4 , respectively, when the MCF was bent. Different from using a switch, the Mea. signal, i.e., combination signal of C₃ and C4, i.e., C34, was simultaneously acquired by using an OC at the time of T_3 , as shown in Fig. 1(c). Obviously, both the data volume and acquisition time could be effectively reduced by using an OC. Therefore, an OC was employed for parallel measurement to achieve fast shape reconstruction [18].

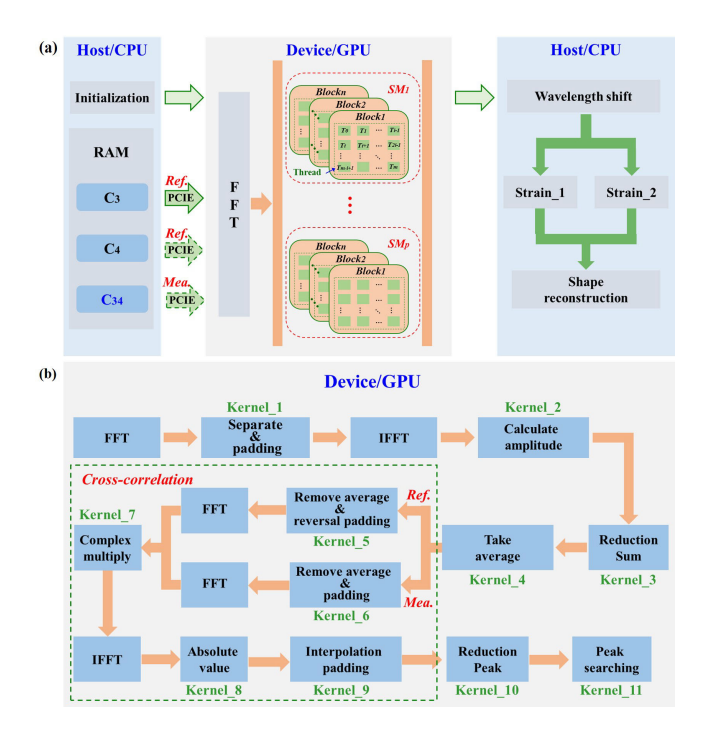
Generally, the Ref. signal, i.e., C_3 and C_4 , and Mea. signal, i.e., C_{34} , were first subjected to fast Fourier transformation (FFT) to convert them from the optical frequency domain to distance domain. Then, the afore-obtained signals were separated into multiple segments of the same size, i.e., Seg¹, Seg², ..., and Segⁿ. In the CPU, the strain distribution



Flowchart of cross correlation wavelength shift of Core3, i.e., C3, and Core4, i.e., C4, of MCF using (a) CPU and (b) GPU, respectively. Note that the collected signals of C3 and C4 are defined as reference (Ref.) signals, when the MCF is straight, i.e., without strain; the measurement (Mea.) signal is defined as the combination signal of C₃ and C₄, i.e., C₃₄, when the MCF is bent. FFT: fast Fourier transformation; IFFT: inverse FFT.

along C3 and C4 was achieved by serially calculating the wavelength shift of each segment, i.e., cycling n times, as shown in Fig. 2(a). In the GPU, the wavelength shift of C_3 , i.e., $\Delta \lambda_1$, $\Delta \lambda_2$, ..., $\Delta \lambda_n$, and C_4 , i.e., $\Delta \lambda_1'$, $\Delta \lambda_2'$, ..., $\Delta \lambda_n'$ was obtained by parallel performing cross correlation between C₃ and C₃₄ and C₄ and C₃₄, respectively. Compared to the CPU, the cross correlation calculations of n segments of C_3 , i.e., Seg_3^1 and Seg_{34}^1 , Seg_3^2 and Seg_{34}^2 , ..., Seg_3^n and Seg_{34}^n , and C_4 , i.e., Seg_4^1 and Seg_{34}^1 , Seg_4^2 and Seg_{34}^2 , ..., Seg_{34}^n and $\operatorname{Seg}_{34}^n$, were performed synchronously in the GPU, as shown in Fig. 2(b). In other words, the strain of C₃ and C₄ needs to be demodulated in the GPU only once. Therefore, the GPU instead of CPU was selected to achieve the calculation of wavelength shift for fast shape reconstruction.

The detailed process to calculate wavelength shift for shape reconstruction was illustrated in Fig. 3. In the CPU side, the initialization operation was first performed to allocate GPU's memory and initialize the demodulation parameters, and then, the Ref. signals of C₃ and C₄ and Mea. signal of C₃₄ were cached in RAM and uploaded to the GPU's memory via PCI express (PCIE), as shown in Fig. 3(a). As shown in Fig. 3(b), in the GPU side, the signal subjected to FFT was separated and padded with zero to size M for each segment using Kernel_1, i.e., Step1. Generally, the data size M was chosen as a power of 2 to maximize the computational efficiency of FFT and inverse FFT (IFFT) in the GPU [19]. Step2, the IFFT was conducted and the amplitude of the complex signal was calculated using Kernel_2. Step3, the reduction method was employed to sum and average each segment of the Ref. and Mea. signal, corresponding to the use of Kernel_3 and Kernel_4, respectively. Step4, the Ref. signal was reversed and padded with zeros to the size of 2M-1 using Kernel 5, while Mea. signal was directly padded with zeros to the same



(a) Software scheme of data parallel computing for shape Fig. 3. reconstruction based on OFDR using CPU and GPU. (b) Flowchart of library and kernel functions in GPU. RAM: random access memory; PCIE: PCI express; SM: streaming multiprocessor.

size using Kernel 6. To improve the correlation between the Ref. and Mea. signal, the remove average method was used to subtract the average of segmented data. It could be given by

$$D^{\text{Ref}'}(i) = D^{\text{Ref}}(i) - \frac{S^{\text{Ref}} + S^{\text{Mea}}}{M}$$

$$D^{\text{Mea}'}(i) = D^{\text{Mea}}(i) - \frac{S^{\text{Ref}} + S^{\text{Mea}}}{M}$$
(2)

$$D^{\text{Mea}'}(i) = D^{\text{Mea}}(i) - \frac{S^{\text{Ref}} + S^{\text{Mea}}}{M}$$
 (2)

where SRef and SMea were the results obtained using the reduction summation method, representing the summation of D^{Ref} and D^{Mea} , which reference and measurement data after taking amplitude, respectively. Step5, the FFT and IFFT were sequentially performed on Ref. and Mea. signal, where the result of FFT was multiplied by Kernel_7 and IFFT was taken an absolute value using Kernel_8. Step6, peak searching was conducted on each segment by Kernel_10 and Kernel_11 that executed with the reduction method, where Kernel 9 was used for zero-padding interpolation to the data size of 2M on each segment to enhance the computational efficiency in reduction method. At this time, the wavelength shift along C_3 and C_4 , corresponding to strain_1 and strain_2, could be calculated by cross correlation operation between C₃ and C₃₄ and C₄ and C₃₄ in the GPU. Obviously, 11 custom kernel functions, i.e., Kernel_1, Kernel_2, ..., and Kernel_11, were all used for parallel computing in the GPU.

As shown in Fig. 3(a), a streaming multiprocessor (SM) consisted of n blocks, i.e., Block₁, Block₂, ..., and Block_n, with one block consisting of m threads, i.e., T_0, T_1, \ldots , and T_m , respectively. Multiple SMs of the GPU, i.e., SM₁, SM_2, \ldots , and SM_p , were run simultaneously in each kernel function. Therefore, a large number of independent threads

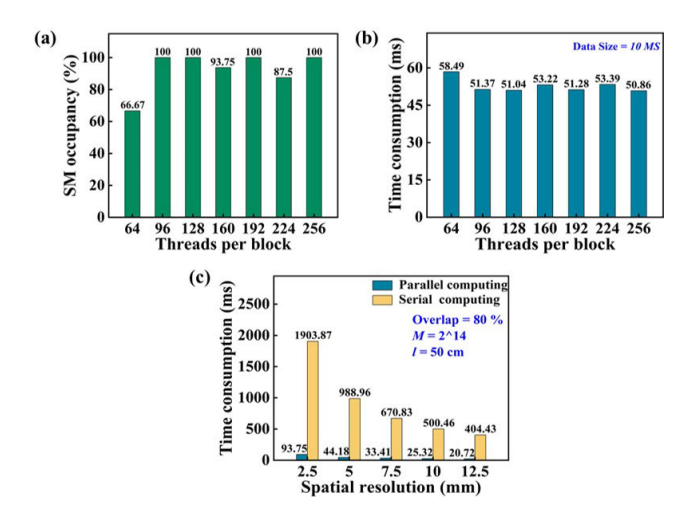


Fig. 4. (a) SM occupancy of kernel functions under different numbers of threads in each block. (b) Time consumption of different threads under the simulated data size of 10 MS. (c) Comparison of time consumption using parallel and serial computing. Note that the number of threads, sliding window overlap rate, size after zero padding, and the length of MCF in (c) are 256, 80%, 2^14, and 50 cm, respectively.

were executed simultaneously to accomplish the parallel computation in the GPU for shape reconstruction [17]. In the GPU, computational efficiency was primarily influenced by the number of threads in a block, which can be reflected in the occupancy rate of the SM. Usually, a warp is 32 threads, which running the same instruction. The relationship between the occupancy rate of SM, i.e., η , and the number of warps could be given by [20]

$$\eta = \frac{W_{\text{active}}}{W_{\text{max}}} = \frac{W_{\text{active}}}{48} \tag{3}$$

where W_{active} and W_{max} are the active and maximum number of warps for each SM, respectively, and $W_{\text{max}} = 48$. Here, the active number of warps, i.e., W_{active} , for each SM could be given by [20]

$$W_{\text{active}} = N_{\text{blocks/SM}} \cdot N_{\text{warps/block}}$$

$$= \min(B_{\text{max}}, \lfloor W_{\text{max}}/(T_m/32) \rfloor) \cdot T_m/32$$

$$= \min(16, \lfloor 48/(T_m/32) \rfloor) \cdot T_m/32. \tag{4}$$

Here, the maximum number of blocks is 16, i.e., $B_{\text{max}} = 16$, and the symbol of [] is the round-down calculation. Based on (4), the occupancy rate of the SM, i.e., η , is only dependent on the number of threads, i.e., T_m . As shown in Fig. 4, the effect of the number of threads in a block on occupancy rate was analyzed and simulated, when the number of threads varied from 64 to 256 with a step of 32. Obviously, the occupancy rate is up to 100% under the number of threads of 96, 128, 192, and 256, respectively, as shown in Fig. 4(a). To obtain the optimal number of threads, the time consumption of different threads per block under the simulated data size of 10 MS was compared, as shown in Fig. 4(b). Obviously, the time consumption was consistent with the occupancy rate, i.e., the higher the occupancy rate, the less consumption time, and the higher the computing efficiency. The occupancy rate and consumption time are 100% and 50.86 ms, when the number of threads is 256.

TABLE I PROCESSED DATA SIZE AND THE NUMBER OF THREADS AND BLOCKS IN EACH KERNEL FUNCTION ($T_m=256$)

Kernel Function	Data Size (D_k)	Number of threads (T_m)	Number of blocks (B_m)
Kernel_1, 2 and 3	пМ	T_m	nM/T_m
Kernel_4	nM/T_m	M/T_m	n
Kernel_5, 6 7 and 8	n(2M-1)	T_m	$\left\lceil n(2M-1)/T_m\right\rceil$
Kernel_9 and 10	2 <i>nM</i>	T_m	$2nM/T_m$
Kernel_11	$2nM/T_m$	$2M/T_m$	n

Furthermore, the number of blocks allocated in each kernel function, i.e., B_m , based on data size and the number of threads could be expressed as

$$B_m = \lceil D_k / T_m \rceil \tag{5}$$

where D_k is the actual data size processed in the kernel functions, and the symbol of $\lceil \rceil$ is the round-up calculation. As previously mentioned, each kernel function is used to process data from two cores simultaneously, and each thread is used to process two data points simultaneously. The processed data size and the number of allocated threads and blocks in each kernel function are listed in Table I. To improve computing efficiency through reduction method, the number of threads in Kernel_4 and Kernel_11 was set to M/T_m and $2M/T_m$, respectively.

To demonstrate the performance of GPU-based OFDR, the effect of spatial resolution on the time consumption was compared using CPU and GPU. Here, only the calculation time in MATLAB and CUDA toolkit is considered as time consumption, ignoring the sweeping time of the TLS. As shown in Fig. 4(c), the time consumption using parallel computing is 93.75, 44.18, 33.41, 25.32, and 20.72 ms at spatial resolutions of 2.5, 5.0, 7.5, 10.0, and 12.5 mm, corresponding to 1903.87, 988.96, 670.83, 500.46, and 404.43 ms using serial computing. Note that the number of threads, window overlap rate, size after zero padding, and the length of MCF are 256, 80%, 2¹⁴, and 50 cm, respectively, i.e., overlap = 80%, $M = 2^{14}$, and l = 50 cm. Obviously, the higher the spatial resolution, the longer the time consumed. Moreover, the time consumption was shortened by nearly 22 times at the spatial resolution of 5 mm, while only about 20 times at the spatial resolutions of 2.5, 7.5, 10.0, and 12.5 mm, and the time consumption of parallel computing is much less than serial computing. Therefore, a spatial resolution of 5 mm was finally selected for subsequent shape reconstruction.

III. EXPERIMENTAL RESULTS AND DISCUSSION

To verify the performance of the GPU-based OFDR system, the 2-D and 3-D shape sensing properties were further investigated. As shown in Fig. 5(a), the MCF was laid on curvature plate with radii of 15.0, 12.5, 10.0, and 7.5 cm, respectively. Note that the length of the reconstructed MCF is

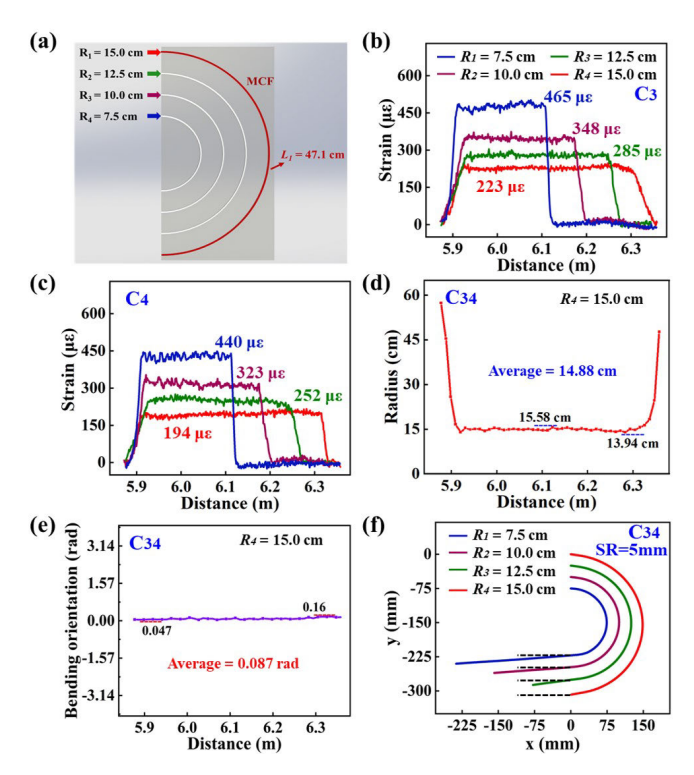


Fig. 5. (a) Schematic of using MCF for 2-D shape sensing; obtained strain distribution of (b) C3 and (c) C4 under the curvature radius of 7.5, 10.0, 12.5, and 15.0 cm, respectively. Calculated (d) curvature radius and (e) bending orientation at the groove curvature radius of 15.0 cm. (f) Reconstructed 2-D shapes with curvature radii of 7.5 cm, 10.0, 12.5, and 15.0, respectively.

set to 47.1 cm, corresponding to the arc length under maximum curvature radius, i.e., $R_4 = 15$ cm. The strain distribution of C_3 and C₄ calculated through flowchart in Fig. 3 was illustrated in Fig. 5(b) and (c). When the curvature radii were 7.5, 10.0, 12.5, and 15.0 cm, the obtained average strains of C₃ were 465, 348, 285, and 223 $\mu\varepsilon$, respectively, corresponding to 440, 323, 252, and 194 $\mu\varepsilon$ of C₄. Note that the spatial resolution, window overlap rate, and data size after zero padding are 5 mm, 80%, and 2¹⁴ based on the previous optimization result, respectively. As shown in Fig. 5(d), the curvature radius derived from C₃₄ using apparent curvature vector method was ranged from 13.94 to 15.58 cm. The average curvature radius, i.e., 14.88 cm, exhibited tiny difference with the setting, i.e., 15.0 cm, and the large curvature radius at the starting and ending section was caused by the mismatch between the fiber and groove diameter [21]. Moreover, the average bending orientation was fluctuated from 0.047 to 0.16 rad, where the average was 0.087 rad, as shown in Fig. 5(e). As shown in Fig. 5(a) and (f), the 2-D shapes of MCF were well reconstructed based on the afore-obtained curvature radius and bending orientation using the Bishop framework [22]. The slight shape deviations observed in the zero-strain region with curvature radii of 7.5, 10.0, and 12.5 cm were due to the slight distortion and outward expansion of MCF when placed in the groove. The reconstruction errors, i.e., the Euclidean distance between the actual and reconstructed end position, were 3.23%, 2.26%, 2.51%, and 2.12%, respectively.

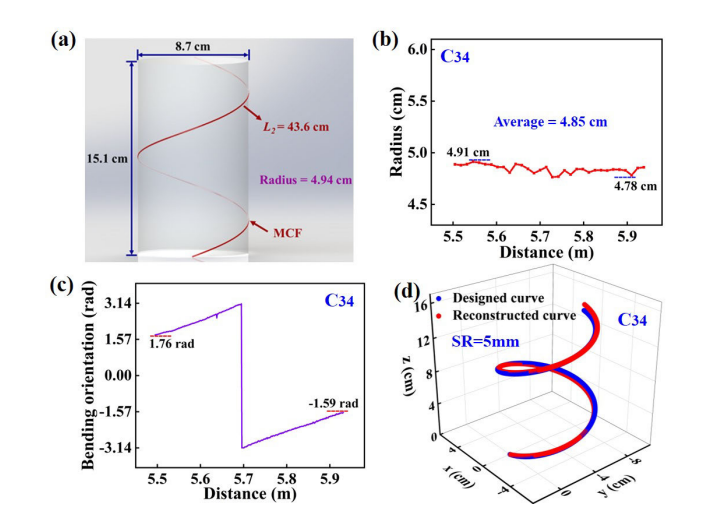


Fig. 6. (a) Schematic of using MCF for 3-D shape sensing; calculated (b) curvature radius and (c) bending orientation based on C34 combination and (d) reconstructed spiral 3-D shape.

TABLE II
TIME CONSUMPTION COMPARISON BETWEEN CPU AND GPU FOR 2-D AND 3-D SHAPE SENSING

Shape		3D			
Method	R_I	R_2	R_3	R_4	S
CPU	942.98	963.68	950.71	962.95	863.84
GPU	42.82	42.64	44.09	43.73	40.12
Times	22.0	22.6	21.6	22.0	21.5

As shown in Fig. 6(a), the MCF was further placed in a spiral groove on the cylinder, where the diameter and height of the cylinder were 8.7 and 15.1 cm, respectively. Similarly, the obtained curvature radius was between 4.78 and 4.91 cm, as shown in Fig. 6(b). The average curvature radius was 4.89 cm, which was 0.05 cm different from the theoretical radius of spiral curve, i.e., 4.94 cm. Moreover, the bending orientation was varied linearly from 1.76 rad to π , $-\pi$ to -1.59 rad, as shown in Fig. 6(c). The reconstructed 3-D shape was also well consistent with the designed spiral curve, as shown by the red and blue curves in Fig. 6(d), where the reconstruction error was 2.47% under the length of 43.6 cm. This indicated that the 2-D and 3-D shape of standard MCF could be well reconstructed using GPU parallel computation.

Moreover, the time consumption of deploying the Bishop reconstruction algorithm on CPU and GPU was compared. The entire reconstruction algorithm deployed on the CPU took 0.77 ms, while performing partial reconstruction algorithm on the GPU cost 1.56 ms. Thus, the Bishop reconstruction algorithm was executed on the CPU. In addition, the time consumption of using CPU and GPU for 2-D and 3-D shape reconstruction was further compared, as shown in Table II. It is obvious that the time consumption of 2-D shape reconstruction is greater than 3-D shape reconstruction due to the used MCF length for 2-D, i.e., 47.1 cm, is longer

than that for 3-D, i.e., 43.6 cm. The time consumption was reduced by nearly 21 times for 2-D and 3-D shape sensing.

IV. CONCLUSION

In this work, a fast shape reconstruction OFDR system that employs GPU to parallelly calculate the cross correlation wavelength shift of the two outer cores of an MCF was proposed and demonstrated. The optical coupler was employed to achieve parallel measurement. The number of threads per block was set 256, where the occupancy rate is 100%, and consumption time under a simulated data size of 10 MS is 50.86 ms. The time consumption of GPU, i.e., 44.18 ms, is much less than CPU, i.e., 988.96 ms, under the spatial resolution and MCF length of 5 mm and 50 cm, respectively. Using GPU parallel computation, the 2-D and 3-D shapes, i.e., wavelength shift of two outer cores of standard MCF, were well reconstructed under the spatial resolution of 5 mm. The reconstruction errors of 2-D shapes, i.e., curvature radii of 7.5, 10.0, 12.5, and 15.0 cm, were 3.23%, 2.26%, 2.51%, and 2.12%, while 2.47% for 3-D spiral shape. Compared to the serial computing with CPU, the time consumption is reduced by nearly 21 times for 2-D and 3-D shape sensing.

ACKNOWLEDGMENT

Rongyi Shan, Yanjie Meng, Huajian Zhong, Wenfa Liang, Shuai Xiao, Yuhao Kong, Zhenwei Peng, Changrui Liao, and Cailing Fu are with Shenzhen Key Laboratory of Photonic Devices and Sensing Systems for Internet of Things, Guangdong and Hong Kong Joint Research Centre for Optical Fibre Sensors, State Key Laboratory of Radio Frequency Heterogeneous Integration, Shenzhen Key Laboratory of Ultrafast Laser Micro/Nano Manufacturing, Key Laboratory of Optoelectronic Devices and Systems of Ministry of Education/Guangdong Province, College of Physics and Optoelectronic Engineering, Shenzhen University, Shenzhen 518060, China (e-mail: 2200453068@email.szu.edu.cn; mengyanjie2020@email.szu.edu.cn; 2250453061@email.szu.edu.cn; 2210452110@email.szu.edu.cn; 1041562932@qq.com; cliao@szu.edu.cn; fucailing@szu.edu.cn).

Zhicai Zhang is with China Nonferrous Metal (Guilin) Geology and Mining Company Ltd., Guilin, Guangxi 541004, China (e-mail: 474253835@qq.com).

Yiping Wang is with Guangdong Laboratory of Artificial Intelligence and Digital Economy (SZ), Shenzhen 518107, China, and also with Shenzhen Key Laboratory of Ultrafast Laser Micro/Nano Manufacturing, Key Laboratory of Optoelectronic Devices and Systems of Ministry of Education/Guangdong Province, College of Physics and Optoelectronic Engineering, Shenzhen University, Shenzhen 518060, China (e-mail: ypwang@szu.edu.cn).

REFERENCES

- Y. Meng et al., "Shape sensing using two outer cores of multicore fiber and optical frequency domain reflectometer," *J. Lightw. Technol.*, vol. 39, no. 20, pp. 6624–6630, Oct. 2021.
- [2] Ł. Szostkiewicz et al., "High-resolution distributed shape sensing using phase-sensitive optical time-domain reflectometry and multicore fibers," Opt. Exp., vol. 27, no. 15, p. 20763, 2019.
- [3] Z. Chen et al., "Demonstration of large curvature radius shape sensing using optical frequency domain reflectometry in multi-core fibers," *IEEE Photon. J.*, vol. 13, no. 4, pp. 1–9, Aug. 2021.
- [4] J. Francoeur et al., "Optical frequency domain reflectometry shape sensing using an extruded optical fiber triplet for intra-arterial guidance," Opt. Exp., vol. 31, no. 1, p. 396, Jan. 2023.
- [5] Y. Guolu, "Optical fiber distributed three-dimensional shape sensing technology based on optical frequency-domain reflectometer," *Acta Optica Sinica*, vol. 42, no. 1, 2022, Art. no. 0106002.

- [6] F. Parent et al., "Enhancement of accuracy in shape sensing of surgical needles using optical frequency domain reflectometry in optical fibers," *Biomed. Opt. Exp.*, vol. 8, no. 4, p. 2210, 2017.
- [7] M. Gherlone, P. Cerracchio, and M. Mattone, "Shape sensing methods: Review and experimental comparison on a wing-shaped plate," *Prog. Aerosp. Sci.*, vol. 99, pp. 14–26, May 2018.
- [8] Y. Tian, H. Dang, W. Liu, J. Cui, Y. Li, and J. Tan, "Structure shape measurement method based on an optical fiber shape sensor," *Meas. Sci. Technol.*, vol. 34, no. 8, Aug. 2023, Art. no. 085102.
- [9] I. Floris, J. M. Adam, P. A. Calderón, and S. Sales, "Fiber optic shape sensors: A comprehensive review," *Opt. Lasers Eng.*, vol. 139, Apr. 2021, Art. no. 106508.
- [10] H. Moon, J. Jeong, S. Kang, K. Kim, Y.-W. Song, and J. Kim, "Fiber-Bragg-grating-based ultrathin shape sensors displaying single-channel sweeping for minimally invasive surgery," *Opt. Lasers Eng.*, vol. 59, pp. 50–55, Aug. 2014.
- [11] X. Bao and L. Chen, "Recent progress in distributed fiber optic sensors," Sensors, vol. 12, no. 7, pp. 8601–8639, Jun. 2012.
- [12] D.-P. Zhou, L. Chen, and X. Bao, "Distributed dynamic strain measurement using optical frequency-domain reflectometry," *Appl. Opt.*, vol. 55, no. 24, p. 6735, 2016.
- [13] Q. Bai et al., "Fast strain measurement in OFDR with the joint algorithm of wavelength domain differential accumulation and local cross-correlation," *J. Lightw. Technol.*, vol. 41, no. 20, pp. 6599–6607, Oct. 2023.
- [14] S. Li et al., "Twist compensated, high accuracy and dynamic fiber optic shape sensing based on phase demodulation in optical frequency domain reflectometry," *Mech. Syst. Signal Process.*, vol. 216, Jul. 2024, Art. no. 111462.
- [15] Z. Sha, H. Feng, Y. Shi, and Z. Zeng, "Phase-sensitive optical time domain reflectometer with ultrafast data processing based on GPU parallel computation," Appl. Opt., vol. 57, no. 10, p. 2679, 2018.
- [16] S. Zhao, J. Cui, L. Suo, Z. Wu, D.-P. Zhou, and J. Tan, "Performance investigation of OFDR sensing system with a wide strain measurement range," J. Lightw. Technol., vol. 37, no. 15, pp. 3721–3727, Aug. 1, 2019.
- [17] C. Wang et al., "GPU-based real-time distributed dynamic strain sensing in optical frequency domain reflectometry," *IEEE Sensors J.*, vol. 21, no. 21, pp. 24166–24176, Nov. 2021.
- [18] Y. Meng et al., "Multicore fiber shape sensing based on optical frequency domain reflectometry parallel measurements," J. Lightw. Technol., vol. 42, no. 10, pp. 3909–3917, May 2024.
- [19] (May 2024). CUDA cuFFT API Reference. [Online]. Available: https://docs.nvidia.com/cuda/cufft/index.html
- [20] (May 2024). CUDA Occupancy Calculator. [Online]. Available: https://xmartlabs.github.io/cuda-calculator/
- [21] C. Fu et al., "OFDR shape sensor based on a femtosecond-laser-inscribed weak fiber Bragg grating array in a multicore fiber," *Opt. Lett.*, vol. 49, no. 5, pp. 1273–1276, 2024.
- [22] C. Fu et al., "High-spatial-resolution φ-OFDR shape sensor based on multicore optical fiber with femtosecond-laser-induced permanent scatter arrays," Opt. Lett., vol. 48, no. 12, pp. 3219–3222, 2023.



Rongyi Shan was born in Guangdong China, in 1999. He received the B.S. degree from Guangdong University of Technology, Guangzhou, China, in 2022. He is currently pursuing the master's degree in optical engineering with Shenzhen University, Shenzhen, China.

His current research interest is distributed optical sensing.



Yanjie Meng was born in Guangling, China, in 1994. He received the M.S. degree from China University of Mining and Technology, Xuzhou, China, in 2019, and the Ph.D. degree in optical engineering from Shenzhen University, Shenzhen, China, in 2023.

His main research interests include optical fiber shape sensing and femtosecond laser processing.



Huajian Zhong was born in Jiangxi, China, in 1998. He received the B.S. degree from Changchun University of Science and Technology, Changchun, China, in 2020. He is currently pursuing the Ph.D. degree in optical engineering with Shenzhen University, Shenzhen, China.

His current research focuses on distributed optical sensing.



Changrui Liao (Member, IEEE) received the Ph.D. degree from Hong Kong Polytechnic University, Hong Kong, in 2012.

He was a Distinguished Professor at the College of Physics and Optoelectronic Engineering, Shenzhen University, Shenzhen, China, and holds the position of the Deputy Director of Guangdong and Hong Kong Joint Research Center for Optical Fiber Sensors and the Director of Shenzhen Key Laboratory of Ultrafast Laser Micro and Nano Manufacturing. Then,

he joined Shenzhen University and successively served as a Lecturer, an Associate Professor, and a Distinguished Professor. His research interests lie in ultrafast laser 3-D nanolithography and its application in optical fiber sensors, smart chips, and new energy. He authored/co-authored two book chapters, >190 journal articles, and >ten patents in 3-D nanolithography and optical fiber sensors. His works were cited >7000 times with an H-index 48 (SCIE).



Wenfa Liang was born in Guangdong, China, in 1999. He received the bachelor's degree from Dongguan University of Technology, Dongguan, China, in 2018.

His research interests include signal demodulation based on FPGA and fiber optic shape sensing.



Shuai Xiao was born in Hengyang, China, in 2001. He received the B.E. degree from Jiangsu Normal University, Xuzhou, China, in 2022.

His main research interest is optical fiber shape sensing.



Cailing Fu was born in Hubei, China, in 1989. She received the M.S. degree in optical engineering from Wuhan Institute of Technology, Wuhan, China, in 2015, and the Ph.D. degree in optical engineering from Shenzhen University, Shenzhen, China, in 2018.

From 2018 to 2020, she was a Postdoctoral Research Fellow with the Information and Communication Engineering, Shenzhen University, where she has been an Associate Professor, since June, 2020. She has authored or

co-authored more than 50 journals and conference papers. Her current research interests focus on distributed optical fiber sensing technology.



Yuhao Kong was born in Qufu, China, in 1999. He received the bachelor's degree from Hefei University of Technology, Hefei, China, in 2022. His main research interest is femtosecond laser processing.



Zhenwei Peng was born in Guangdong China, in 1999. He received the B.S. degree from Changchun University of Science and Technology, Changchun, China, in 2021.

His current research interest is fiber Bragg grating array.



Yiping Wang (Senior Member, IEEE) was born in Chongqing, China, in 1971. He received the B.Eng. degree in precision instrument engineering from Xi'an Institute of Technology, Xi'an, China, in 1995, and the M.S. and Ph.D. degrees in optical engineering from Chongqing University, Chongqing, in 2000 and 2003, respectively.

From 2003 to 2005, he was a Postdoctoral Fellow with Shanghai Jiao Tong University, Shanghai, China. From 2005 to 2007, he was a Postdoctoral Fellow with Hong Kong Polytech-

nic University, Hong Kong. From 2007 to 2009, he was a Humboldt Research Fellow with the Institute of Photonic Technology (IPHT), Jena, Germany. From 2009 to 2011, he was with the Optoelectronics Research Center (ORC), University of Southampton, Southampton, U.K., as a Marie Curie Fellow. Since 2012, he has been with Shenzhen University, Shenzhen, China, as a Distinguished Professor. He has authored or co-authored one book, 21 patent applications, and more than 240 journals and conference papers. His current research interests include optical fiber sensors, fiber gratings, and photonic crystal fibers.

Prof. Wang is a Senior Member of the Optical Society of America and the Chinese Optical Society.

Zhicai Zhang, photograph and biography not available at the time of publication.